# Analysis of the temporal and spectral output properties of a mode-locked and *Q*-switched laser oscillator with a nonlinear mirror based on stimulated Brillouin scattering

P. Kappe, R. Menzel, and M. Ostermeyer*
*Institute for Physics, Nonlinear Optics, University of Potsdam, Am Neuen Palais 10, 14469 Potsdam, Germany*
(Received 27 March 2006; published 20 July 2006)

The emission dynamics of a mode-locked laser oscillator with a nonlinear mirror based on stimulated Brillouin scattering (SBS) has been investigated with regard to its spectrum and to its intensity distribution. The investigation was carried out experimentally as well as by numerical simulations. The laser yields trains of pulses with measured durations of 410 ps and energies of the single pulse of up to 2 mJ. Two theoretical models describing the complex emission dynamics of a mode-locked SBS-laser oscillator are introduced. The first model consists of spectrally resolved laser rate equations and thus describes the mode locking in the frequency domain by the superposition of the longitudinal resonator modes. The SBS-*Q*-switch is incorporated by a phenomenological description of the time dependent SBS reflectivity. Numerical simulations based on this model yield the evolution of a few 100 longitudinal laser modes and the corresponding intensity distribution during the course of a *Q*-switch pulse with 10-ps resolution. The influences of the different components on the spectrum and thus on the pulse duration will be discussed. The second model describes all occurring dynamics in the time domain providing easy access to the study of misalignment on the output dynamics. Results of numerical simulations of both models and measurement results are compared.

DOI: 10.1103/PhysRevA.74.013809 PACS number(s): 42.55.Rz, 42.65.Es, 42.65.Sf

## I. INTRODUCTION

Simultaneous *Q* switching (QS) and mode locking (ML) of a laser oscillator, also referred to as transient mode locking (or QML), yields trains of ultrashort pulses during a *Q*-switch pulse envelope. Compared to a simple *Q* switch QML leads to considerably higher peak powers and in contrast to the cw-mode-locking can still issue pulse energies in the mJ range. It is thus a very elegant way to combine high pulse energies with ps-pulse durations from a laser oscillator.

The first report on simultaneous mode locking and *Q* switching was published in 1965 by Mocker and Collins [1]. They used a saturable absorber to mode lock and *Q* switch a ruby laser. Using saturable absorbers QML often occurred when cw-mode-locking was actually desired and is in that case also referred to as *Q*-switching instabilities. Thus limits that separate the ML from the QML regime are well investigated [2,3].

Today $Cr^{4+}$:YAG crystals sometimes bonded to the amplifier crystal [4] and semiconductors are often applied for *Q* switching and also the simultaneous mode locking of Nd lasers [5–7]. Also nonlinear mirrors typically on the basis of second harmonic generation (SHG) and a dichroic mirror can be exploited to provide a ML or QML operation [7,8]. Lamb and Damzen used a passive external cavity [9] and a regenerative amplifier [10] consisting of a conventional mirror and a nonlinear mirror on the basis of the stimulated Brillouin scattering (SBS) to generate bandwidth and to mode lock the output from a narrow bandwidth pulsed oscillator.

The laser to be discussed in this paper is a self-starting SBS-laser oscillator where the SBS mirror provides passive *Q* switching. The mode-locking inherent to the SBS [11,12] was supported by acousto optic modulation in an additional component. In the following two sections the laser setup and its general output properties will be summarized and experimental results relating to the observation of the *Q* switching will be presented. In Secs. IV and V two models to describe the laser output dynamics are introduced. In the first model the laser rate equations are applied for all longitudinal resonator modes individually while all modes share the stored inversion in the homogeneously broadened Nd:YAG. The numerical solution of these equations yield the evolution of the longitudinal modes. Consequentially the output dynamics on the ps time scale can be calculated from the spectrum of these modes.

The second model describes all dynamics solely in the time domain. The propagation of a pulse in the resonator is considered and all changes that the pulse experiences during each round trip are recorded. A similar approach has been taken by Kuizenga and Siegman [13,14]. They found an analytical description for steady state mode locking by pursuing the changes to a pulse during one resonator roundtrip and demanding no net change. Since we are interested in the QML regime we have to numerically calculate a large number of roundtrips. The SBS-*Q* switch will be taken into account by a phenomenological description that is identical for both models. We assume an intensity dependent generation of an overall sound wave amplitude in the SBS mirror that determines its effective SBS reflectivity. In Sec. VI results from numerical simulations based on the two models are presented and used to discuss the influences of modulation depth, modulation frequency detuning, SBS Stokes shift, SBS-*Q* switch parameters, and the starting conditions on the QML dynamics and the transient spectrum.

## II. SBS-LASER OSCILLATOR SETUP

The reflectivity of a nonlinear SBS mirror stems from coherent scattering of light at an acoustic sound wave grat-

*Electronic address: oster@uni-potsdam.de

 

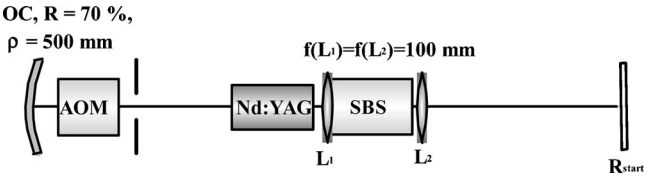


FIG. 1. SBS-laser setup

ing. Due to the movement of the acoustic wave the reflected light experiences a Doppler shift to lower frequencies that amounts to the resonance frequency of the acoustic wave—the so called Brillouin frequency $\nu_B$. The process starts from acoustic noise in the SBS material [15]. The incident light will scatter from random sound waves which in turn will be amplified by the beat mode pattern of the incident and the back-reflected light via electrostriction. This feedback mechanism is the reason for the nonlinear behavior of the SBS reflectivity. However, the amplification depends on the overlap of the two light waves and becomes maximal for a phase conjugating reflection. This leads to a preferred generation of a phase conjugatingly reflecting sound wave and in fact SBS mirrors show high fidelity phase conjugating behavior [16]. Applied in a laser oscillator or in a double pass MOPA laser their phase conjugating reflection leads to a compensation of, e.g., thermally induced phase distortions and hence prevents beam quality degradation at high powers [17].

For low intensity incident light waves the SBS mirror is virtually transparent. A threshold of incident pulse energy has to be overcome until the SBS reflection becomes significant. This means that a simple resonator consisting of an SBS mirror and a conventional reflector is not self-starting and has to be either pumped by an external light source or embedded in a conventional start resonator where the oscillation can be initiated.

A schematic of the setup of the SBS laser to be discussed here is shown in Fig. 1. Its general output properties have been presented in detail in [18]. The SBS laser consists of two coupled cavities. The conventional start resonator is given by the output coupler (OC) and the start resonator mirror $R_{\text{start}}$. The nonlinear SBS mirror and the OC form the SBS resonator. The SBS mirror consists of a gas cell containing $SF_6$ at a pressure of 20 bar and is situated in the center of the start resonator. Active support of the SBS-inherent mode locking is provided by an acousto optic modulator (AOM) which is placed in front of the OC.

For the layout of the resonator several aspects have to be considered: As mentioned before the SBS-reflected light experiences a frequency shift. So if this light should be still accommodated in the resonator the shift in frequency must be an integer multiple of the resonator's longitudinal mode spacing. In other words the resonator length has to be a multiple of a fundamental resonator length, the Brillouin length $L_B$ which corresponds to the Brillouin frequency $\nu_B$ by $L_B=c/2\nu_B$. The Brillouin frequency for $SF_6$ at 20 bar is 240 MHz so that the Brillouin length is 62.5 cm in this case.

The second aspect to be considered relates to the mode locking. If active mode locking is desired the resonator's longitudinal mode spacing has also to be tuned to the modulation frequency of the AOM. In this case it is 80 MHz leading to a fundamental resonator length according to the mode locking of 187.5 cm. Since this is exactly three times the Brillouin length the resonator length tuning for the SBS is always given if the mode-locking condition is fulfilled.

For optimal mode locking this requirement has to be met by both resonators, the SBS resonator as well as the start resonator. The matching of the longitudinal mode spacing of the start resonator is in this case also vital for the SBS-Q switching: The SBS threshold for $SF_6$ is too large to accomplish a self-starting SBS process in an oscillator from the acoustic noise [19]. An initial sound wave has to be built up in the SBS material by Brillouin enhanced four wave mixing (BEFWM) [20] of the back and forth traveling waves in the start resonator. The result can be a considerable reduction of the SBS threshold for the incident light if again a multiple of the longitudinal mode spacing of the start resonator modes matches the Brillouin frequency of the SBS material. We chose the optical SBS-resonator length to equal the fundamental mode-locking resonator length of 187.5 cm and the start resonator to have twice this length.

## III. GENERAL OUTPUT PROPERTIES

The laser head used in the setup described above is a flash lamp-pumped Nd:YAG rod with a diameter of 6.35 mm with pump pulse energies of up to 11 J and repetition rates of up to 1 kHz. The oscillation begins in the start resonator when the SBS mirror is still transparent. With the leading edge of the first spike in the start resonator the sound wave is created by BEFWM. Once the sound wave grating is initiated it is effectively amplified by SBS and the SBS reflectivity increases quickly. With increasing SBS reflectivity the oscillation switches from the start resonator to the SBS resonator. Because the SBS reflectivity can reach very high values (close to unity) and also because losses due to the phase distortions in the pumped laser rod are prevented by the phase conjugating reflection of the SBS mirror the SBS-resonator quality is very high. The start resonator quality in contrast is chosen to be low so that the switch from start resonator to SBS resonator is also a switch of quality. This passive $Q$-switching behavior can be influenced by tuning the start resonator loss which in this case is achieved by an alteration of the start resonator mirror reflectivity. The higher the loss in the start resonator the longer it takes until the lasing threshold is reached during the pump process. Thus there will be more gain accumulated in the laser active material when the pulse finally starts with a spike in the start resonator. So an SBS laser with higher start resonator losses issues shorter $Q$-switch pulses of higher energy with longer time intervals between two pulses whereas for a low loss start resonator the pulses come in quick succession and will be of long duration and low energy.

Figure 2 illustrates the measured intensity distribution of the mode-locked SBS laser. The top graph shows a typical $Q$-switch pulse burst. Here the signal of the flash lamp-pump pulse is superimposed to the signal of the pulses. The apparent difference in amplitude of the pulse stems from a digitizing effect in the display of the short pulses on a compara-

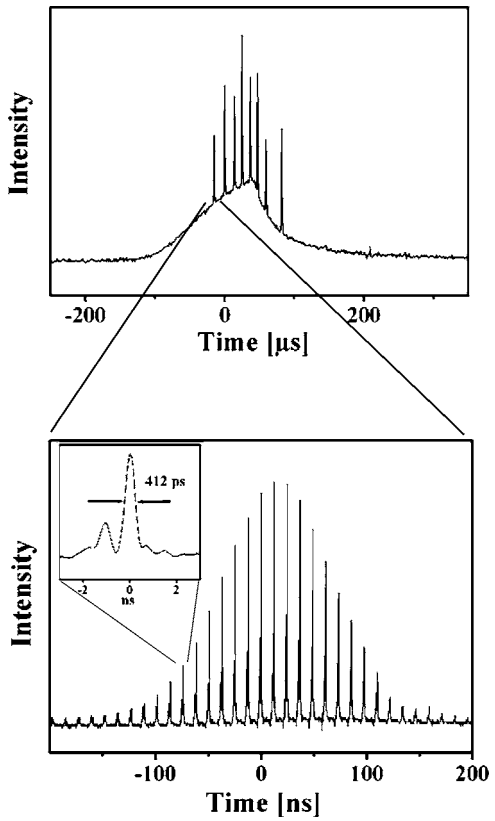


FIG. 2. Emission dynamics; top: $Q$-switch pulse train superimposed to flash lamp-pump pulse, bottom: mode locked pulse train underneath $Q$-switch pulse envelope.

tively long time scale. The bottom graph represents the mode-locked dynamics of a single $Q$-switch pulse.

Bursts of up to seven pulses could be generated within a pump pulse duration of 300 $\mu$s for an $R_{start}$=0.88. The output power ranged between 2.0 W for one pulse per burst and 2.7 W for seven pulses. In both cases transverse fundamental mode operation is achieved. In the latter case the $Q$-switch pulse energy was 2.3 mJ, the pulse duration full width at half maximum (FWHM), was 117 ns. For $R_{start}$=0.32 one single pulse was received from each pump pulse. The output power equals 2 W leading to a $Q$-switch pulse energy of 11 mJ (see also Fig. 9). Additional active mode locking did neither influence the $Q$-switch-pulse duration nor the $Q$-switch pulse energy significantly.

The output properties of the laser such as temporal $Q$-switch pulse spacing, pulse duration, and pulse energy are coupled: By changing the start resonator loss all these parameters are altered dependently. But by additionally varying the pump parameters free parameters are added and the mentioned output parameters can within boundaries be arbitrarily chosen. The large variability of this laser's temporal output properties was exploited for fundamental research in materials processing [21].

The switch from start resonator to SBS resonator can be directly observed if we look at the starting edge of the pulse [22]. As long as the oscillation occurs in the start resonator we find a 40 MHz periodicity in the output signal of the laser. The oscillation in the SBS resonator in contrast shows

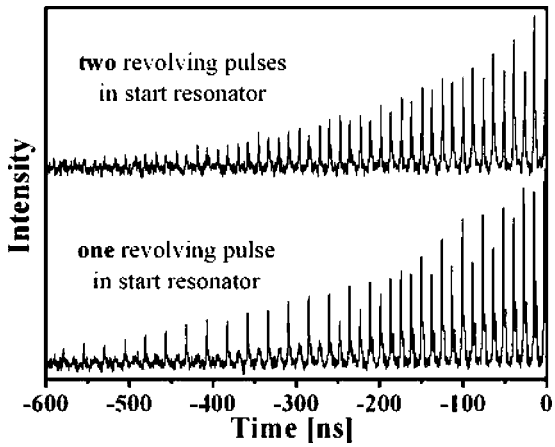


FIG. 3. $Q$-switch observation, two different cases.

a 80 MHz periodicity and it is most apparent if the laser is mode locked. Figure 3 depicts the leading edge of the $Q$-switch pulse of the mode-locked laser. In the bottom graph the transition from the 40 to 80 MHz can be clearly seen which corresponds to a single pulse that starts to revolve in the start resonator and than gradually switches to the SBS resonator due to the increasing SBS reflectivity. Thus we can conclude that the on switching of the SBS reflectivity takes about 300–400 ns. Since the AOM consistently works with 80 MHz frequency its loss vanishes twice during each start resonator roundtrip. Accordingly, two pulses that are spaced by a half of the roundtrip time can coexist in the start resonator. If both pulses resemble in amplitude the switching is not apparent from the periodicity of the output signal (top graph in Fig. 3). The most likely case to encounter, however, is a mixture of both cases: Two pulses with different amplitudes resulting in a 40 MHz superstructure to the 80 MHz repetition rate.

If mode locking is applied we receive trains of ps pulses with repetition rates of 80 MHz where the envelope of the pulse train is shaped by the $Q$ switch (bottom graph in Fig. 2). The pulse energy of the ps pulses is influenced by the start resonator reflectivity $R_{start}$ for two reasons. First, the $Q$-switch pulse energy increases with decreasing $R_{start}$. Second, the $Q$-switch pulse width decreases with decreasing $R_{start}$. So the $Q$-switch pulse energy is split into the smaller number of ps pulses the lower $R_{start}$. Both effects lead to an increase of ps pulse energy with decreasing $R_{start}$. The ps-pulse energy ranges from 0.2 to 2 mJ for start resonator reflectivities of 0.88 down to 0.32, respectively.

The upper limit for the single pulse duration was directly measured with a fast photodiode (Thorlabs SV2) and an oscilloscope with 2 GHz bandwidth (Tectronix TDS 794D) to be 412 ps (see Fig. 2). For the highest achieved pulse energy of 2 mJ this results in a peak power of almost 5 MW. The $M^2$-number of the laser was determined with a beam propagation analyzer (Spiricon $M^2$-200) to be better than 1.4.

## IV. SPECTRALLY RESOLVED LASER RATE EQUATIONS

The laser rate equations are coupled differential equations to describe the evolution of the photon density and the inver-

sion density and their mutual interactions inside the cavity. They are the means of choice to calculate laser output dynamics [23]. However, the obtained photon density as a function of time is in fact the mean photon density inside the resonator. Therefore dynamics on a time scale shorter than the resonator roundtrip time cannot be resolved and additional efforts have to be made in order to display mode-locking behavior in the calculations. The envelope of a mode-locked pulse is on one hand determined by its mode spectrum and on the other by the phase relations of the respective modes. To comprise the mode-locking dynamics in the simulation the laser's spectrum and its transient behavior have to be included in the modeling. The spectrum can be considered by solving the laser rate equation for the photon density for each of the longitudinal modes individually. The laser rate equation for the photon density $\phi_n$ of the $n$th mode of a mode-locked four-level laser neglecting the population of the pump band and the lower laser level is

$$\frac{d\phi_n}{dt} = -\frac{\phi_n(t)}{\tau_R} + \frac{l}{L}\frac{n_2(t)\sigma_n}{\tau_{sp}} + \frac{l}{L}n_2(t)\sigma_n\phi_n(t) + [-2\phi_n(t) + \phi_{n+1}(t) + \phi_{n-1}(t)]m\frac{c}{2L}. \quad (1)$$

Here $\tau_R$ is the resonator decay time, $l$ the length of the laser active material, $L$ the resonator length, $n_2$ the population density of the upper laser level, and $\sigma_n$ the frequency dependent stimulated emission cross section of the upper laser level. The first term on the right-hand side of Eq. (1) denotes the resonator losses followed by the terms for the amplification and the spontaneous emission. The third term describes an exchange of population between spectrally adjacent modes resulting from the modulation of depth $m$.

To include the nonlinear SBS mirror into this model several aspects have to be considered. First of all with increasing reflectivity of the SBS mirror the oscillation switches from the start resonator to the SBS resonator. This switch affects on the one hand the length and on the other hand the loss of the resonator that the revolving light experiences. Therefore we have to substitute the resonator decay time $\tau_R$ and the resonator length $L$ by corresponding expressions that depend on the time-dependent reflectivity of the SBS-mirror $R_{SBS}(t)$:

$$\frac{l}{L} \rightarrow \left\{ R_{SBS}(t)\frac{l}{L_{SBS}} + [1 - R_{SBS}(t)]\frac{l}{L_{start}} \right\} \quad (2)$$

$$\frac{1}{\tau_R} \rightarrow \left\{ \frac{R_{SBS}(t)}{\tau_{SBS}} + \frac{[1 - R_{SBS}(t)]}{\tau_{start}} \right\}. \quad (3)$$

$L_{SBS}$, $L_{start}$, $\tau_{SBS}$, $\tau_{start}$ are the lengths and decay times for the SBS—and the start resonator, respectively.

Furthermore the Stokes shift, which the reflected light experiences due to the movement of the reflecting sound wave, has to be considered. The Stokes shift for $SF_6$ at a pressure of 20 bar amounts to 240 MHz. This value is exactly three times the spectral spacing of the longitudinal modes of the SBS resonator. Neglecting anti-Stokes- and higher Stokes-orders we can describe the Stokes shift as a transfer of energy down the longitudinal mode scale of the SBS resonator by three steps:

$$\frac{d\phi_n}{dt}(stokes\ shift) = [\phi_{n+3}(t) - \phi_n(t)]R_{SBS}(t)\frac{c}{2L_{SBS}}. \quad (4)$$

Including (2)–(4) into (1) we obtain for the time derivative of the photon density of the $n$th mode:

$$\begin{aligned}\frac{d\phi_n}{dt} = &-\left\{ \frac{R_{SBS}(t)}{\tau_{SBS}} + \frac{[1 - R_{SBS}(t)]}{\tau_{start}} \right\}\phi_n(t) \\ &+ \left\{ R_{SBS}(t)\frac{l}{L_{SBS}} + [1 - R_{SBS}(t)]\frac{l}{L_{start}} \right\}\frac{n_2(t)\sigma_n}{\tau_{sp}} \\ &+ \left\{ R_{SBS}(t)\frac{l}{L_{SBS}} + [1 - R_{SBS}(t)]\frac{l}{L_{start}} \right\}n_2(t)\sigma_n\phi_n(t)c \\ &+ [-2\phi_n(t) + \phi_{n+1}(t) + \phi_{n-1}(t)]m \\ &\times \frac{c}{2\{R_{SBS}(t)L_{SBS} + [1 - R_{SBS}(t)]L_{start}\}} \\ &+ [\phi_{n+3}(t) - \phi_n(t)]R_{SBS}(t)\frac{c}{2L_{SBS}}. \end{aligned} \quad (5)$$

Strictly speaking this description only applies for those modes which can be accommodated in both resonators equally. The SBS-resonator modes are spaced by 80 MHz whereas the modes of the start resonator which is twice as long are spaced by 40 MHz. Only every second start resonator mode will fit into the SBS resonator. For the numerical calculations the improper start-resonator modes will not be considered at all.

Due to the homogeneously broadened amplification bandwidth of Nd:YAG the sum over all modes can be utilized to calculate the time derivative of the population of the upper laser level:

$$\frac{dn_2}{dt} = W_p n_0 - n_2 c\sum_n \phi_n\sigma_n - \frac{n_2}{\tau_2}. \quad (6)$$

$W_p$ denotes the pump rate and $n_0$ and $n_2$ are the density of dopant atoms and the population density of the upper laser level. It remains to implement the time-dependent reflectivity $R_{SBS}(t)$ of the SBS mirror. There is a model of the sound wave generation and the resulting reflectivity with temporal and spacial resolution for an external SBS reflection [24–26]. But we could not find any published model describing the sound wave generation and reflectivity with spacial resolution for the more complex case of an SBS mirror inside a cavity. Here, we confine ourselves to a phenomenological description of the generation and decay of an overall sound wave amplitude $Q(t)$ in the SBS cell and its corresponding reflectivity $R_{start}(t)$:

$$\frac{dQ}{dt} = -\frac{Q(t)}{\tau_p} + g * I(t) \quad (7)$$

$$R_{SBS}(t) = 1 - \exp(-Q(t)/Q_s). \quad (8)$$

Equation (8) is a more or less arbitrarily chosen function ranging from zero to unity describing the saturation behavior of the SBS reflectivity. $\tau_p$ is the phonon lifetime, $Q_s$ represents the saturation sound wave amplitude, and we call $g^*$ the extended Brillouin gain. Whereas the simple Brillouin gain $g$ is a material constant $g^*$ encompasses the focusing conditions as well. $g^*$ and $Q_s$ will be used to fit the shape of the calculated $Q$-switch pulse envelopes to the experimental results. Their magnitudes determine if a $Q$-switch pulse occurs at all and govern the slope of the SBS reflectivity. The latter influences the leading edge of the $Q$-switch pulse envelope. They do not influence the time at which the pulse occurs and therefore the pulse duration and pulse energy significantly. Also there is no direct relation to the mode locking. A third parameter that is used to fit the calculation to the experiment is the linear loss factor $V$ of the SBS resonator. It governs the resonator decay time and therefore the final edge of the pulse.

The resulting electrical field $E(t)$ is obtained by the summation of the field contributions of all modes $(E_n(t) \sim [\phi(t)]^{0.5})$ assuming that the phase factors are identical for all modes and can hence set to be zero. In this case the intensity $I(t)$ is given by:

$$I(t) = |[E_1(t)e^{i\omega_1 t} + \cdots \cdot \cdot + E_n(t)e^{i\omega_n t}]|^2. \tag{9}$$

The assumption that the phase factors for all modes are zero is identical to assuming perfect mode locking. In this case the resulting mode-lock pulse is transform limited by the spectrum. Phase noise due to spontaneous emission and the SBS bandwidth as well as a mismatch between longitudinal mode spacing and modulation frequency are being neglected.

Another aspect that is not incorporated in this model is the propagation of the light in the resonator. If we would start a calculation according to this model with just one mode occupied it would yield three modes populated for the next time step due to the exchange term for the modulation. In the next but one time step already five modes would be populated notwithstanding the fact that the light would actually have to do one full roundtrip until it passes the modulator for a second time. The same argument applies for the Stokes shift as well what becomes most apparent when $R_{SBS}$ becomes unity. In this case all the light will be shifted by three modes for each roundtrip thus the spectrum is expected to be shifted as a whole and the Stokes shift would not contribute to the generation of bandwidth in reality. In this model, however, the Stokes shift is described as an exponential decay and growth where a constant percentage of the population of the respective mode is shifted in each time step. As we will see in Sec. VI this description yields a generation of bandwidth even though $R_{SBS}$ approaches unity.

In the following we will refer to this model based on spectrally resolved rate equations as the frequency domain model since the mode-locking dynamics are described in the frequency domain.

## V. DESCRIPTION OF THE OUTPUT DYNAMICS IN THE TIME DOMAIN

The description of the mode locking in the frequency domain as presented in Chap. IV yields dynamics on a ps time scale that are strictly related to the spectrum of the intensity. It is a best case scenario since imperfections such as frequency mismatches and phase noise due to the statistical spontaneous emission process are left out. This section offers a model with a contrary approach by describing all occurring dynamics in the time domain. Spontaneous emission is assumed to be continuous wave and the mode-locking effect of the AOM is incorporated as a harmonic loss modulation. To display subroundtrip time dynamics a spacial resolution of the intensity along the axis of the resonator is introduced. Due to the propagation of the light this is equivalent to a temporal resolution.

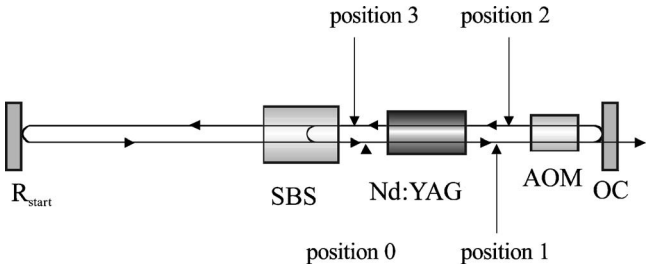


FIG. 4. Time domain calculation scheme.

The basic idea of this model is to display the intensity at one certain spot in the resonator, i.e., position 0 in Fig. 1 in contrast to the mean intensity in the resonator that is considered in the rate equations. In order to compute the intensity $I(t)$ at a certain time $t$ we refer to the intensity $I(t\text{-}T)$ that was to be found here one roundtrip time $T$ ago and calculate all changes that the light has experienced during this roundtrip. In order to calculate the changes during this roundtrip three intermediate steps will be taken corresponding to the positions 1–3 in the resonator indicated in Fig. 4.

The first step would be to calculate the amplified intensity $I_1$ and the depleted inversion density $n_2'$ after the first pass of the amplifier:

$$I_1 = I_0(t-T)\exp[n_2(t)\sigma l] + n_2\frac{\sigma}{\tau_2}, \tag{10}$$

$$n_2' = n_2(t) - \tfrac{1}{2}n_2(t)\sigma I_0(t-T)\Delta t. \tag{11}$$

The expression for the inversion depletion is derived from the laser rate equations. The factor $\frac{1}{2}$ owes to the fact that forward and backward traveling light is considered in two different steps. $\Delta t$ refers to the width of the time step that is calculated. The second step describes the harmonic loss modulation and linear resonator as well as output coupling losses:

$$I_2 = I_1\left[1 - m\frac{\sin(\varpi_{AOM}t) + 1}{2}\right]^2 VR_{OC}. \tag{12}$$

$\omega_{AOM}$ is the modulation frequency of the AOM, $V$ the resonator roundtrip loss factor, and $R_{0C}$ the output coupling reflectivity. What follows is a second pass through the amplifier now with the partially depleted inversion population $n_2'$.

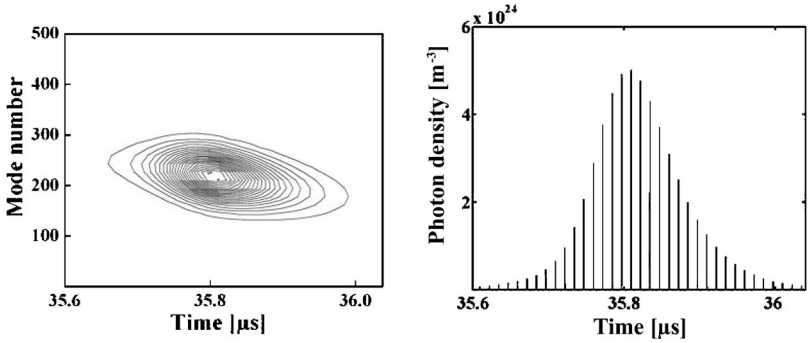


FIG. 5. Transient spectrum and intensity distribution from frequency domain model for spontaneous emission into all modes.

$$I_3 = I_2 \exp[n_2'(t)\sigma l] + n_2' \frac{\sigma}{\tau_2}. \quad (13)$$

In the calculation of the inversion population for the next time step $n_2(t+\Delta t)$ expressions for the pump process and the spontaneous emission loss must be included:

$$n_2(t+\Delta t) = n_2' + \left[ -\frac{1}{2} n_2' \sigma I_2 - n_2' \frac{\sigma}{\tau_2} + W_p n_0 \right] \Delta t. \quad (14)$$

Now we can obtain the intensity $I_0$ at the examined position by considering the transmission of the SBS mirror in both directions:

$$I_0(t) = I_3 R_{SBS}(t) + I_{start}(t-T) R_{start} V_{start}. \quad (15)$$

$I_{start}$ is the portion of the light that leaks through the SBS mirror into the start resonator:

$$I_{start}(t) = [1 - R_{SBS}(t)] I_3. \quad (16)$$

Apparently the propagation described by this model approximates the experimental setup described in Fig. 1. This model describes a setup with the amplifier and the modulator situated at the position of the output coupler. So pumping and depletion by other fractions of the revolving light between the first and second pass through the amplifier remains unconsidered. Also the influence of the Stokes shift on the mode locking is not taken into account.

## VI. NUMERICAL SIMULATIONS

Now the two models will be applied to explain different aspects of the emission dynamics. The numerical solution of the spectrally resolved laser rate equations was done by the Euler method. The simulations with both models were implemented with MATLAB on a conventional personal computer. For both models the starting conditions were zero intensity in the resonator and a completely depleted laser material. So the buildup of inversion was displayed from its very beginning. The pumping conditions were chosen according to the experiment described in Sec. III but any time dependence of the pump power during the flash lamp-pump pulse is neglected. The average power during the flash lamp pump pulse was 60 kW and the excitation efficiency was estimated to be 5%. Considering the rod dimensions of 10 cm in length and 6.35 mm in diameter and the dopant density of 1.38 $10^{23}$ cm$^{-3}$ this yields a pump rate of $W_p$=36.7 Hz. The pump duration until the first pulse occurs ranges from 20 to 80 $\mu$s depending on $R_{start}$.

Since we desire to display the laser dynamics on a ps time scale this demands a very high number of steps within the overall period of several 10 $\mu$s to be calculated. In addition for the frequency domain model the effort scales with the number of considered modes that was typically 300–500. To limit the time expanse for the simulation of one pump—pulse cycle to a reasonable duration the step width was maintained variably. During the buildup of inversion the step width is chosen wider ($10^{-10}$ s) for the frequency domain model and as soon as the intensity in the start resonator becomes appreciable the step width is set smaller ($10^{-11}$ s) to fully display the mode-locking dynamics. Under these conditions a full simulation of a period of 100 $\mu$s corresponding to 1–5 $Q$-switch pulses takes about 2 h. In the time domain model the calculation of each time step consists of only a small number of fundamental computations so the same time span can be calculated with a $10^{-11}$ s resolution within a few seconds and without the need of a variable step width. In order to ascertain that numerical inaccuracies are negligible the temporal resolution was enhanced by a factor of 10 and still the same results were gained.

Figure 5 shows the results of a simulation of the development of 501 modes and the corresponding intensity for a start resonator mirror reflectivity $R_{start}$=0.75. The maximum of the stimulated emission cross section profile is located on mode number 251. The left hand part of Fig. 5 shows the dynamics in the population of the 501 modes as a contour plot with lines of equal intensity. The bandwidth of the calculated emission is dominated by the spontaneous emission profile and is in this case independent of the modulation depth $m$. The shift to lower frequencies that the spectrum experiences in the course of the pulse is caused by the SBS Stokes shift.

The right hand part of Fig. 5 displays the calculated distribution of the intensity showing a 100% modulation contrast with a period of 12.5 ns corresponding to the roundtrip time and the longitudinal mode spacing of the SBS resonator.

Indeed we know from earlier experiments [18] that for the case without active mode locking only every third mode with a spectral spacing of 240 MHz is populated. The 240 MHz periodicity in the spectrum corresponds to the Brillouin frequency of $SF_6$. The omittance of two out of three modes indicates that the bandwidth of the spectrum in this case is generated by the Stokes shift and originates from just one dominant mode. Accordingly we will choose spontaneous emission into just one mode to be the starting conditions in the following simulations.

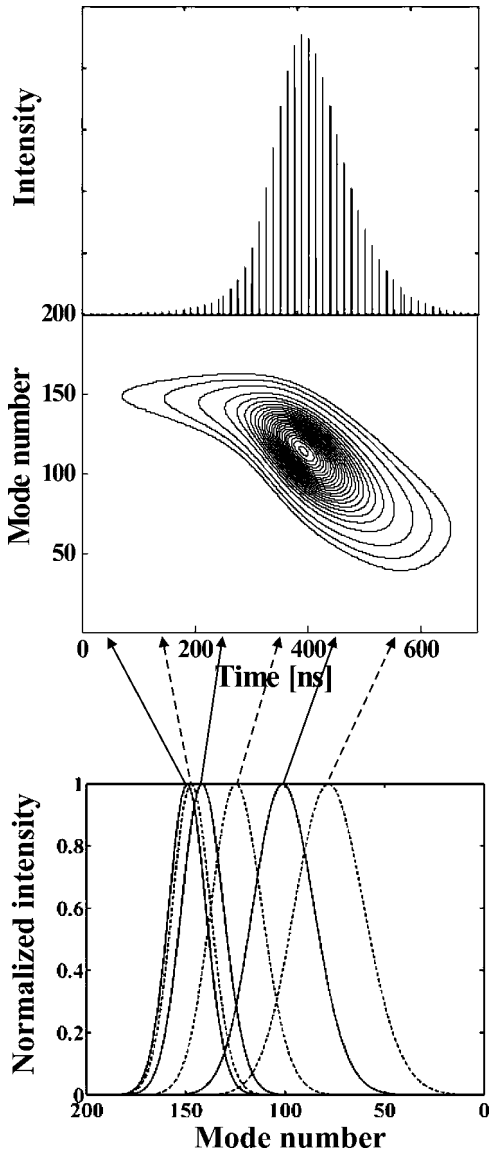


FIG. 6. Intensity distribution (top), transient spectrum (middle), and several sectional views (bottom) for spontaneous emission into one mode.

The top part of Fig. 6 shows the intensity distribution. The corresponding transient spectrum resulting from a simulation of the development of 301 modes while only the 151th mode is fed by spontaneous emission is depicted in the midsection of Fig. 6. The bottom graph depicts sectional views from the transient spectrum at times indicated by the arrows. For comparison reasons the intensity in the respective spectra is normalized to unity. It can be clearly seen that at the starting edge of the pulse the shift of the maximum of the emission spectrum as well as the increase in bandwidth is still small due to the small $R_{SBS}$ and accelerates and finally saturates in the course of the pulse. As already indicated in the introduction of the model in Sec. IV the generation of bandwidth by the Stokes shift does not cease with $R_{SBS}$ approaching unity (see Table I) which is due to the approximated implementation of the Stokes shift in the model. The Stokes shift is described as an exponential decay and transfer of the population of the modes according to the roundtrip time and $R_{SBS}$ rather than a discrete shift after exactly one SBS-resonator roundtrip.

TABLE I. Emission bandwidths corresponding to the sectional views of Fig. 6.

| Time [ns] | Bandwidth [GHz] |
|---|---|
| 50 | 1.78 |
| 150 | 1.83 |
| 250 | 2.04 |
| 350 | 2.45 |
| 450 | 2.90 |
| 550 | 3.31 |

Whereas in the case of spontaneous emission into all modes the gain profile determined the resulting emission bandwidth now it is governed by the bandwidth generation

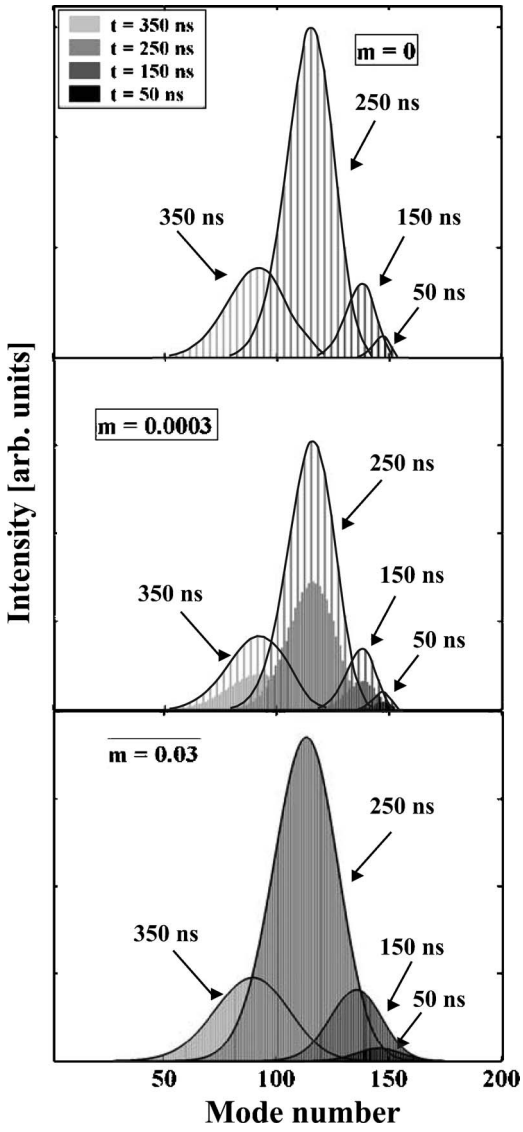


FIG. 7. Calculated spectra for different modulation depths and times within the $Q$-switch pulse.

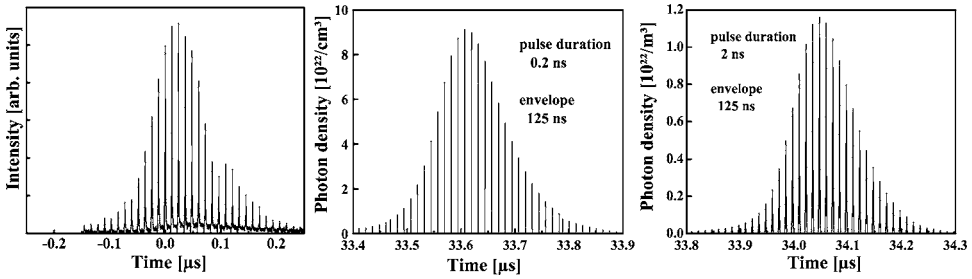


FIG. 8. Pulse structure gained from experiment (left), frequency domain model (middle), and time domain model (right).

of the SBS Stokes shift. The loss modulation by the AOM still does not contribute very much to the generation of bandwidth since it merely provides an exchange of population between spectrally adjacent modes (Fig. 7). Only in the very starting edge of the pulse the spectrum is notably wider if modulation is applied.

Figure 7 shows calculated spectra for different times within the $Q$-switch pulse. For a clearer distinction between the different spectra their envelopes have been added in the display. In the top diagram of Fig. 7 there is no AOM loss modulation applied in the calculation and accordingly only every third mode is populated starting with the initially triggered mode number 151. In the central diagram of Fig. 7 the 240 MHz periodicity caused by the Stokes shift is still apparent. Here a modulation depth of $m=0.0003$ is just enough to allow for a population of the interstitial modes of half the strength of the dominant modes. The modulation depth applied in the experiments was measured to be up to 3% depending on the chosen carrier level (CL) of the AOM.

We can now compare the calculated intensity runs for the two models with each other and with the measurement (Fig. 8). In the calculations as well as in the experiment the reflectivities of the start resonator mirror $R_{start}$ and the output coupler $R_{OC}$ were 75 and 70%, respectively. The linear loss factor $V$ for the resonator roundtrip was 0.95 and the modulation depth $m$ was 0.03 in both simulations.

In terms of $Q$-switch pulse shape and duration there is an excellent correspondence between the two simulations and they are in very good agreement with the measurement. Both simulations yield pulse durations (FWHM) of 125 ns compared to 105 ns in the measurement. The $Q$-switch pulse shape could be slightly influenced by the free parameters $Q_s$ and $g^*$ that govern the slope and the amplitude of $R_{SBS}(t)$. Also the delay time until the $Q$-switch sets is in very good agreement between both models. For the measurement this time is not comparable due to the time dependent pump intensity that is not incorporated into the model.

The correspondence with regard to pulse duration between simulations and experiment can be even improved by taking into account a linear loss factor $V_{start}$ for the start resonator roundtrip to the models. Figure 9 shows the dependence of the $Q$-switch pulse duration on $R_{start}$ for the measurement as well as for the simulations. Choosing $V_{start}$ to be 0.8 the measured dependence of the pulse durations can be well reproduced by the calculations. The reason for the increase in pulse duration with increasing $R_{start}$ is the decrease in the delay time between the beginning of the pumping and the onset of the $Q$-switch pulse which results in a higher gain at the time of the occurrence of the pulse. The calculated delay times for $V_{start}=1$ are also given in Fig. 9. The experimental delay times are left out here because they vary form pulse to pulse owing to the time dependent pump intensity of the flash lamps.

Regarding the mode-lock pulse duration the correspondence between both models and the measurement is poor. The time domain model yields pulse durations of 2 ns while according to the frequency domain model the pulses last for only 0.2 ns. In the experiment we found the pulses to be as short as 0.4 ns. The differences in this regard can be explained by the different assumptions and negligences that are found in the descriptions of the mode locking in both models. In the time domain model the influence of the SBS

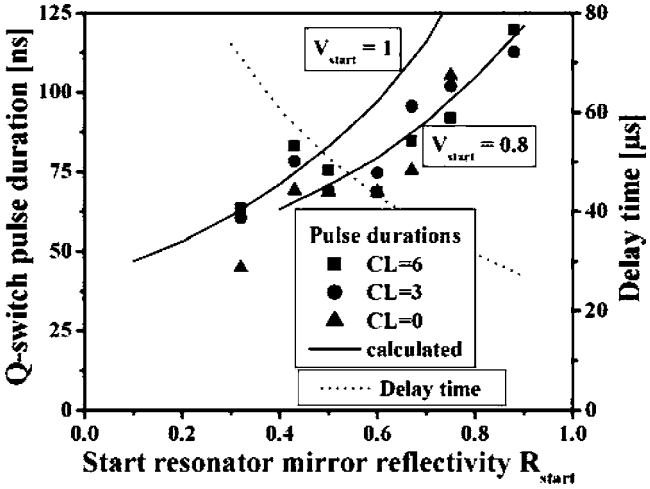


FIG. 9. Dependence of $Q$-switch pulse width and delay time on start resonator quality by measurement and calculation.

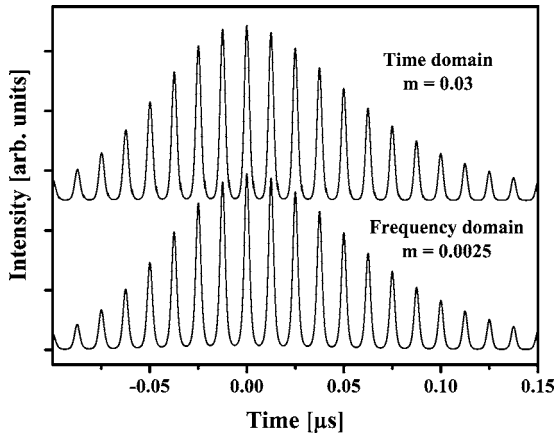


FIG. 10. Comparison of the two models for the $Q$-switch pulse buildup in a conventional mode locked laser.

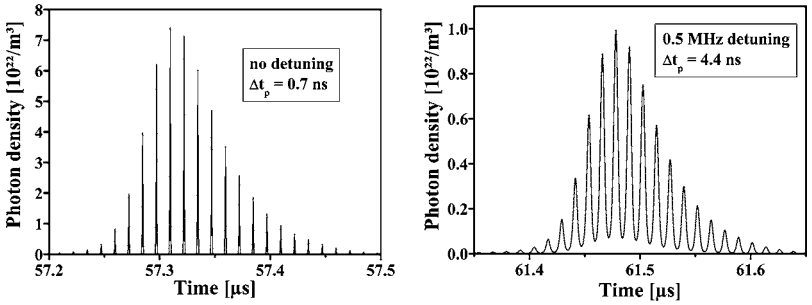


FIG. 11. Intensity from time domain model without detuning (left) and with 0.5 MHz detuning (right).

Stokes shift on the mode locking is not taken into account. As discussed earlier this is the dominant effect for the generation of bandwidth and thus neglecting it leads to considerably longer pulse durations than found in the experiment. The frequency domain model in contrast implies constant and identical phase factors for all modes neglecting phase noise which results in a somewhat optimistic calculation if short pulses are desired.

The main distinguishing aspect for the two models that leads to a difference in the resulting pulse durations by an order of magnitude is the consideration of the contribution of the Stokes shift in the frequency domain approach and its neglect in the time domain model. So for a conventional mode-locked laser the differences in the modeling results should disappear. For a modulation depth of $m=0.03$ we obtain a pulse duration of 1.1 ns from the frequency domain model. The implementation of the loss modulation of the AOM is carried out differently in the two models. Thus, identical results are expected if the differences in the mode-locking descriptions and their underlying assumptions are compensated by an adaptation of the value for the depth of modulation for the two complementary approaches. Figure 10 shows an example where both models issue identical results with regard to the mode-lock pulse duration as well as for the $Q$-switch envelope. This was achieved by choosing a modulation depth for the frequency domain simulation of $m=0.0025$.

To overcome the imperfections inherent to both complementary models it would be desirable to combine the virtues of both models thereby receiving a complete description of the temporal and spectral dynamics. One possible approach would be to merge both models and calculate the evolution

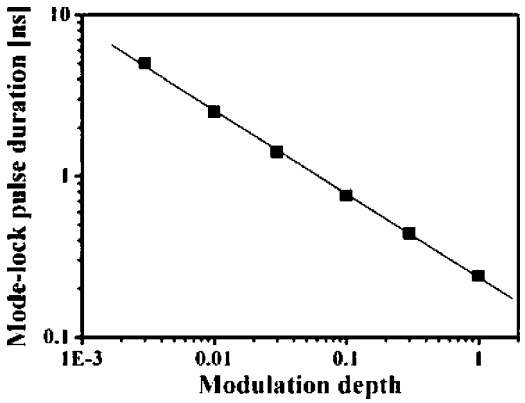


FIG. 12. Dependence of mode lock pulse duration on modulation depth in time domain model.

of the individual modes according to the time-domain model. This, however, would inevitably issue ps dynamics of the individual modes which violates the Heisenberg's uncertainty relation considering the limited bandwidth of the individual modes. A second approach could be the implementation of the Stokes shift into the time domain model. This would demand a more sophisticated description of the movement of the SBS sound wave that would allow to display its phase modulating properties. To implement the phase modulation the electrical fields would have to be considered instead of the intensities and a key virtue of the time-domain model—its simplicity—would get lost. Thus, we decided to work with these two complementary but reasonably simple models, to investigate different aspects of our SBS-mode-locked laser oscillator.

Assuming constant and identical phase factors for all modes a misfit between modulation frequency and resonator roundtrip time that would lead to a divergence of phases cannot be taken into account in the frequency domain model. In the time domain model, however, the effect of maladjustment in frequencies on the pulse structure can be displayed. If the modulation frequency matches the pulse repetition rate the minimum loss of the AOM coincides with the pass of the revolving pulse. Both edges of the pulse experience higher losses compared to the peak of the pulse and thus the pulse is shortened each roundtrip. For a mismatch this is not the case.

A comparison of the intensity distribution for the ideal laser setup with a detuned laser setup gained from a simulation based on the time domain model is given in Fig. 11. Here $m$ was chosen to be 0.1 and $R_{start}$ to be 0.43 which explains the considerably shorter durations of the pulses and the envelope, respectively, compared to the results shown before. The detuning between longitudinal mode spacing and modulation frequency amounts to 0.5 MHz which corresponds to a detuning of the resonator length of 1.2 cm. Whereas the calculation of the ideal setup yields mode-lock pulse widths of 0.7 ns the detuned laser issues pulses with durations of 4.4 ns and the peak power is smaller by a factor of 8 compared to the ideal setup. Because of the higher losses caused by the misfit of the frequencies the $Q$-switch pulse occurs 4 $\mu$s later for the detuned laser.

The effect of the depth of loss modulation on the duration of the mode-lock pulses can also be conveniently studied in the time domain model since other effects are negligible in this picture. Figure 12 shows the results of a calculation that explored this dependence. Here $m$ was varied between 0.3% and unity while all other parameters were held constant. In the double logarithmic display of Fig. 12 the result can be well fit by a straight line so the dependence of the pulse

duration $\Delta t_{ML}$ on the modulation depth $m$ can be described by $\Delta t_{ML} \propto m^{-0,52}$ which is in very good agreement with analytical calculations that predict an exponent of −0.5 for the QML regime [27] in contrast to −0.25 for the steady state mode locking [13].

## VII. SUMMARY

We presented two theoretical models to describe the output dynamics of a mode-locked SBS laser in the frequency domain and time domain, respectively. A phenomenological description of the passive SBS-Q switch is implemented in both models. Results from numerical simulations applying both models perfectly correspond with measurements with regard to $Q$-switch pulse properties. Standing alone both models are incomplete in the display of the mode-locking behavior. For the frequency domain model the assumption of perfect phase synchronization and for the time domain model the neglect of the SBS Stokes shift can be identified as the major inaccuracies. However, due to their highly complementary approach both models add up to a universal tool to study the influences on the complex dynamics of this laser and of course both concepts are applicable to other systems, i.e., saturable absorber mode locking as well.


[1] H. W. Mocker and R. J. Collins, Appl. Phys. Lett. **7**, 270 (1965).
[2] F. X. Kärtner, L. R. Brovelli, D. Kopf, M. Kampf, I. Calasso, and U. Keller, Opt. Eng. **34**, 2024 (1995).
[3] C. Hönninger, R. Paschotta, F. Morier-Genoud, M. Moser, and U. Keller, J. Opt. Soc. Am. B **16**, 46 (1999).
[4] L. Zhang, D. Li, Q. Zhang, C. Li, Z. Wei, B. Feng, P. Fu, and Z. Zhang, Opt. Commun. **250**, 174 (2005).
[5] Y. F. Chen and S. W. Tsai, IEEE J. Quantum Electron. **37**, 580 (2001).
[6] Y. F. Chen, K. F. Huang, S. W. Tsai, Y. P. Lan, S. C. Wang, and J. Chen, Appl. Opt. **40**, 6038 (2001).
[7] T. M. Jeong, K. S. Kim, C. J. Kim, and C. H. Nam, J. Korean Phys. Soc. **35**, 290 (1999).
[8] P. K. Datta, S. Mukhopadhyay, and S. K. Das, Opt. Express **12**, 4041 (2004).
[9] M. J. Damzen, R. A. Lamb, and G. K. N. Wong, Opt. Commun. **82**, 337 (1991).
[10] R. A. Lamb and M. J. Damzen, J. Opt. Soc. Am. B **13**, 1468 (1996).
[11] B. S. Kawasaki, D. C. Johnson, Y. Fujii, and K. O. Hill, Appl. Phys. Lett. **32**, 429 (1978).
[12] V. N. Lugovoi, IEEE J. Quantum Electron. **19**, 764 (1983).
[13] D. J. Kuizenga and A. E. Siegman, IEEE J. Quantum Electron. **6**, 694 (1970).
[14] A. E. Siegman and D. J. Kuizenga, Appl. Phys. Lett. **14**, 181 (1969).
[15] G. C. Valley, IEEE J. Quantum Electron. **22**, 704 (1986).
[16] A. M. Scott, Opt. Commun. **45**, 127 (1983).
[17] M. Ostermeyer and R. Menzel, Opt. Commun. **171**, 85 (1999).
[18] P. Kappe, M. Ostermeyer, and R. Menzel, Appl. Phys. B **80**, 49 (2005).
[19] H. Meng and H. J. Eichler, Opt. Lett. **16**, 569 (1991).
[20] A. M. Scott and K. D. Ridley, IEEE J. Quantum Electron. **25**, 438 (1989).
[21] M. Ostermeyer, P. Kappe, R. Menzel, S. Sommer, and F. Dausinger, Appl. Phys. A **81**, 923 (2005).
[22] M. Ostermeyer, K. Mittler, and R. Menzel, Phys. Rev. A **59**, 3975 (1999).
[23] A. E. Siegman, *Lasers* (University Science Books, Sausalito, CA, 1986), Chap. 24.
[24] R. Menzel and H. J. Eichler, Phys. Rev. A **46**, 7139 (1992).
[25] S. Afshaarvahid, A. Heuer, R. Menzel, and J. Munch, Phys. Rev. A **64**, 043803 (2001).
[26] S. Afshaarvahid and J. Munch, J. Nonlinear Opt. Phys. Mater. **10**, 1 (2001).
[27] D. J. Kuizenga, D. W. Phillion, T. J. Lund, and A. E. Siegman, Opt. Commun. **9**, 221 (1973).